



# HHS Public Access

Author manuscript

*Nat Biomed Eng.* Author manuscript; available in PMC 2019 December 01.

Published in final edited form as:

*Nat Biomed Eng.* 2019 June ; 3(6): 427–437. doi:10.1038/s41551-019-0371-x.

## Detection of unamplified target genes via CRISPR–Cas9 immobilized on a graphene field-effect transistor

Reza Hajian<sup>1</sup>, Sarah Balderston<sup>1</sup>, Thanhtra Tran<sup>1</sup>, Tara deBoer<sup>2</sup>, Jessy Etienne<sup>2</sup>, Mandeep Sandhu<sup>1</sup>, Noreen A. Wauford<sup>2</sup>, Jing-Yi Chung<sup>2</sup>, Jolie Nokes<sup>3</sup>, Mitre Athaiya<sup>1</sup>, Jacobo Paredes<sup>4</sup>, Regis Peytavi<sup>5</sup>, Brett Goldsmith<sup>3</sup>, Niren Murthy<sup>2</sup>, Irina M. Conboy<sup>2</sup>, and Kiana Aran<sup>1,2,5,\*</sup>

<sup>1</sup>Keck Graduate Institute, The Claremont Colleges, Claremont, CA, USA.

<sup>2</sup>Department of Bioengineering, University of California, Berkeley, Berkeley, CA, USA.

<sup>3</sup>Cardea Bio, San Diego, CA, USA.

<sup>4</sup>Tecnun, School of Engineering, University of Navarra, San Sebastián, Spain.

<sup>5</sup>Nanosens Innovations, San Diego, CA, USA.

### Abstract

Most methods for the detection of nucleic acids require many reagents and expensive and bulky instrumentation. Here, we report the development and testing of a graphene-based field-effect transistor that uses clustered regularly interspaced short palindromic repeats (CRISPR) technology to enable the digital detection of a target sequence within intact genomic material. Termed CRISPR–Chip, the biosensor uses the gene-targeting capacity of catalytically deactivated CRISPR-associated protein 9 (Cas9) complexed with a specific single-guide RNA and immobilized on the transistor to yield a label-free nucleic-acid-testing device whose output signal can be measured with a simple handheld reader. We used CRISPR–Chip to analyse DNA samples collected from HEK293T cell lines expressing blue fluorescent protein, and clinical samples of

Reprints and permissions information is available at [www.nature.com/reprints](http://www.nature.com/reprints).

\* kiana\_aran@kgi.edu. Correspondence and requests for materials should be addressed to K.A.

Author contributions

R.H. optimized the CRISPR–Chip design, performed the CRISPR–Chip DMD experiments, data collection and analysis, LOD optimization, HEK–BFP calibration methodologies in the presence and absence of contamination, and kinetic analysis, and prepared the manuscript. S.B. assisted in optimization of the CRISPR–Chip assay protocols, performed the MB–dRNP studies, DMD patient sample analysis, HEK–BFP PCR experiments and analysis, and prepared the manuscript. T.T. assisted with the initial CRISPR–Chip design, performed initial CRISPR–Chip protocols for HEK–BFP studies, and prepared the manuscript. T.d. performed the synthesis of sgRNA for the *bfp* and Scram studies, genomic purification and initial system design, and helped with manuscript preparation. J.E. contributed to the design of the DMD-based validation of CRISPR–Chip and provided the PCR and sequencing data for the DMD studies. M.S. contributed to the design of the DMD-based validation of CRISPR–Chip and assisted in manuscript preparation. N.A.W. and J.-Y.C. assisted T.D. with the synthesis of sgRNAs for *bfp* studies and assisted with sample preparation. J.N. and B.G. assisted with CRISPR–Chip data analysis and manuscript preparation. M.A. and J.P. assisted with manuscript preparation and data analysis. R.P. assisted with the design of threshold experiments, data analysis and CRISPR–Chip validation. N.M. supervised the synthesis of sgRNAs for the *bfp* and Scram studies. I.M.C. assisted with technology design, DMD validation and manuscript preparation. K.A. designed and developed the technology, planned and supervised the project, analysed, interpreted and integrated the data, and prepared the manuscript.

Competing interests

K. A. is a co-founder of Nanosens Innovations, and R.P. is Vice President of Technology Development in the same company. The other authors declare no competing interests.

Additional information

Supplementary information is available for this paper at <https://doi.org/10.1038/s41551-019-0371-x>.

DNA with two distinct mutations at exons commonly deleted in individuals with Duchenne muscular dystrophy. In the presence of genomic DNA containing the target gene, CRISPR–Chip generates, within 15 min, with a sensitivity of 1.7 fM and without the need for amplification, a significant enhancement in output signal relative to samples lacking the target sequence. CRISPR–Chip expands the applications of CRISPR–Cas9 technology to the on-chip electrical detection of nucleic acids.

---

In recent years, whole-genome sequencing has allowed for the broad analysis and identification of biomarkers indicative of various pathologies<sup>1–3</sup>. This expanded knowledge has allowed for the development of various target-specific nucleic acid detection tools<sup>4–6</sup>. Such tools hold the power to provide physicians with actionable information to improve patient outcomes and introduce precise medical treatment approaches. Most established methods for nucleic acid-based molecular diagnostic tests, such as PCR, have been optimized over the past 30 years to amplify and detect targeted genome sequences<sup>7,8</sup>. Despite significant advancement in nucleic acid detection technologies, the majority of these nucleic acid detection tools are time consuming and costly to use, as they require multi-step reactions, many reagents, trained personnel and complex instrumentation. In addition, quantitative analysis of these nucleic acid amplification techniques often requires sophisticated probe/primer design and optimization methodologies for efficient targeting. Furthermore, they often still rely on large and expensive optical components for detection<sup>9,10</sup>. Therefore, new methodologies are needed to overcome the limitations associated with conventional nucleic acid detection strategies to afford low-cost and fully integrated compact nucleic acid-based diagnostic tools to expand their clinical utility.

In recent studies, clustered regularly interspaced short palindromic repeats (CRISPR)-associated nuclease (Cas)-based methodologies have been utilized to improve on conventional nucleic acid targeting for optical detection<sup>11–13</sup>. CRISPR–Cas proteins, guided by a single-stranded RNA, are a powerful tool for sequence-specific targeting and detection. For example, in 2017, Gootenberg et al.<sup>11</sup> reported the development of the SHERLOCK methodology, which utilized an RNA-guided RNA targeting Cas13a (CRISPR-associated nuclease 13a) to provide a fluorescent signal readout after Cas13a complex hybridization with its target sequence, once initially amplified by recombinase polymerase amplification (RPA). Soon after, the HOLMES methodology was reported by Li et al.<sup>12</sup>, which utilized a DNA-targeting Cas12a to eliminate the need for the DNA to RNA conversion required by SHERLOCK for DNA sequence detection. Both SHERLOCK and HOLMES allowed for the sequence-specific detection of DNA and RNA via collateral cleavage of a single-stranded nucleic acid probe post-amplification<sup>14</sup>. Due to the programmability of CRISPR–Cas RNA guides<sup>15</sup>, these methodologies are easily modified to detect different targets. However, they still rely on initial amplification steps via RPA and T7 transcription, resulting in added time and reagents.

Here, we report the design and construction of a CRISPR-enhanced graphene-based field-effect transistor (gFET) termed CRISPR–Chip. This biosensor combines the gene-targeting capacity of CRISPR–Cas9 with the sensitive detection power of a gFET<sup>16,17</sup> to afford the facile, rapid and selective detection of a target sequence contained within intact genomic

DNA (Fig. 1). CRISPR–Chip, a three-terminal gFET, uses functionalized graphene as a channel between the source and drain electrodes. The graphene is functionalized with a catalytically deactivated Cas9 (dCas9) CRISPR complex, denoted as dRNP, which interacts with its target sequence by scanning the whole genomic sample, unzipping the double helix and associating upstream of a protospacer adjacent motif<sup>18</sup> until it finds and binds to the target sequence that is complementary to the single-guide RNA molecule (sgRNA) within the dRNP<sup>19,20</sup>. The selective hybridization of the target DNA to the dRNP complex modulates the electrical characteristics of the gFET and results in an electrical signal output.

The power of the CRISPR–Chip system is due to the combination of its two main components: the dRNP and the graphene. The immobilized dRNP is not only sequence specific, but also programmable. For example, to expand the scope of CRISPR–Chip analysis to a wide variety of genes, the target-specific 20-nucleotide sequence of the sgRNA within the dRNP construct can be simply modified at the 5' end<sup>15</sup>. The graphene, with a high carrier mobility ( $> 2,000 \text{ cm}^2 \text{ Vs}^{-1}$ ) is sensitive to the adsorption and interaction of charged molecules at its surface<sup>21</sup>. Thus, the hybrid graphene-CRISPR construct of CRISPR–Chip makes it an ideal candidate for next-generation nucleic acid biosensors.

A schematic of the gFET construct of CRISPR–Chip is shown in Fig. 2a. CRISPR–Chip utilizes a liquid-gate electrode, which is in constant contact with the genomic sample contained within the reaction buffer. The applied voltage between the liquid-gate and source electrodes ( $V_g$ ) controls the current flowing between the source and the drain electrodes of the graphene channel. The hybridization of the negatively charged DNA target and immobilized dRNPs on the surface of the graphene channel not only alters the channel conductivity, but also creates an ion-permeable layer atop the graphene surface due to an accumulation of counter ions to maintain charge neutrality. This difference in the concentration of ions between the bulk solution and the immobilized ion-permeable layer creates a Donnan potential<sup>22,23</sup>. This additional potential results in an alteration in the electric field between the source and the gate electrodes, resulting in further modulation of the graphene channel current, enabling sensing beyond the Debye screening length<sup>24–26</sup>. A detailed description of the device operation and measurement method is provided in the Supplementary Information (Device Operation, Measurement Description and Supplementary Figs. 1–6).

CRISPR–Chip is fabricated in several stages using conventional microelectromechanical systems<sup>27</sup> processing and is then functionalized according to the scheme shown in Fig. 2b. Briefly, after fabrication and packaging, the chips are cleaned, and noncovalently functionalized with the molecular linker, 1-pyrenebutanoic acid (PBA), via  $\pi$ - $\pi$  aromatic stacking<sup>21</sup>. Then, dCas9 is immobilized on the surface of the graphene channel via carbodiimide crosslinking chemistry<sup>28,29</sup>. dCas9 immobilization is then followed by surface blocking, with amino-PEG5-alcohol and ethanolamine hydrochloride, to prevent the non-specific adsorption of charged molecules<sup>30–32</sup>. Finally, the immobilized dCas9 is complexed with a sgRNA, specific to a DNA target, forming the anchored dRNP complex.

## Results

### Specificity of the immobilized dRNP to its target sequence

CRISPR–Chip’s binding specificity to its target double-stranded DNA (dsDNA) was first evaluated by utilizing a PCR product of the *bfp* gene, which encodes for blue fluorescent protein, a commonly used gene for CRISPR–Cas gene editing validation<sup>33,34</sup>. A schematic of this experiment is shown in Fig. 3a, where CRISPR–Chips were functionalized with either dRNPs specific to *bfp* (dRNP-BFP) or a scramble dRNP specific to the gene *pcsk9* (ref. <sup>35</sup>) (dRNP-Scram), as described above. *bfp* amplicons were obtained via PCR amplification of genomic DNA from HEK293T cells that had been transfected with a *bfp*-containing lentivirus<sup>34,36</sup>. Non-transfected HEK293T cells are referred to as HEK and *bfp* transfected HEK293T cells are referred to as HEK-BFP cells hereafter. The dRNP-BFP- and dRNP-Scram-functionalized CRISPR–Chips were calibrated, then incubated with 1800 ng of *bfp* amplicons. The sensor response was monitored in real-time and the sensor data were analysed according to equation (1), where  $I_{ds}$  is the current between the drain and source electrodes after incubation with the genomic sample and subsequent washing (see Device Operation in the Supplementary Information for the  $I_{ds}$  equation) and  $I_{ds0}$  is the calibration baseline signal taken in assay buffer during calibration. This calibration step helps to eliminate the effect of sensor-to-sensor variation in resistance, as well as the effect of the buffer. We utilized percent ‘*I* response’ as our unit of measure. *I* response is the percentage change in  $I_{ds}$  (measured after incubation with the sample and the rinsing step) compared with the calibration baseline ( $I_{ds0}$ ).

$$I \text{ response}(\%) = \frac{100(I_{ds} - I_{ds0})}{I_{ds0}} \quad (1)$$

Figure 3b shows the *I* response of the two CRISPR–Chips in the presence of the target *bfp* sequence. CRISPR–Chip functionalized with dRNPs-BFP presented a significantly larger signal than that of the non-specific dRNP-Scram-functionalized CRISPR–Chips ( $P = 0.0002$ ). This result indicates that CRISPR–Chip’s signal output is specific to the immobilized dRNP complex. Furthermore, the real-time monitoring of the CRISPR–Chip response, shown in Fig. 3c, shows CRISPR–Chip’s fast response time (within 2.5 min) in the presence of target dsDNA. CRISPR–Chip specificity was also validated utilizing dRNP-Scram-functionalized CRISPR–Chips after exposure to Scram target amplicons, further showing the specificity of the anchored dRNPs to their target (Supplementary Figs. 8 and 9).

### Affinity of the immobilized dRNP to its target sequence within intact genomic DNA

The ultimate goal of CRISPR–Chip was to detect its target dsDNA sequence from whole-genome samples. Therefore, we first ensured that immobilized dRNPs were capable of binding and maintaining their affinity to the target sequence within the scale of whole-genome samples. For this experiment, the dRNP-BFP complex was immobilized on the surface of carboxylated magnetic beads (MBs) (1  $\mu\text{m}$ ; Invitrogen) with a protocol similar to that of CRISPR–Chip functionalization (Fig. 4a). Briefly, dCas9 was covalently bound to the carboxylated MBs via carbodiimide crosslinking chemistry, blocked and incubated with

sgRNA specific to *bfp* to form the dRNP-BFP complex on the surface of the MBs. The MBs were then incubated with unamplified whole genomic BFP samples obtained from HEK-BFP cell lysate and subsequently extracted using a magnetic separator. The supernatant, which contained any unbound genomic material, was then evaluated using gel electrophoresis (Supplementary Figs. 10) and the concentration of the genomic material was evaluated pre- and post-incubation with MBs to determine the capture efficiency and the relative affinity of the immobilized dRNPs to their target DNA contained within the whole genome. As a negative control, dRNP-BFP-functionalized MBs were incubated with non-target genomic material obtained from HEK cells.

Figure 4b shows that the capture efficiency of the functionalized MBs for the HEK-BFP genomic sample was significantly higher ( $P=0.002$ ) than that of the negative control. These results suggest that the interaction between dRNPs and their target sequences within the full-scale genomic DNA was maintained during the physical force of washing and pipetting when anchored to a surface.

### **CRISPR–Chip capacity for the detection of non-amplified target sequence in the absence and presence of genomic contamination**

Next, we investigated CRISPR–Chip’s ability to detect whole-genome samples containing the *bfp* target. The selection of this genomic BFP model was based on of the experimental evidence collected from the aforementioned PCR model, which demonstrated that the dRNP-BFP-functionalized CRISPR–Chip was able to specifically detect *bfp* amplicons. To investigate CRISPR–Chip ability to detect the *bfp* gene within whole-genome samples, dRNP-BFP-functionalized CRISPR–Chips were fabricated and evaluated in the presence of varying concentrations of the target HEK-BFP genomic samples (300–1,200 ng). For control experiments, dRNP-BFP-functionalized CRISPR–Chips were incubated with 900 ng of HEK genomic sample, which lacked the *bfp* gene. A schematic of this experiment is shown in Fig. 5a. Figure 5b shows that CRISPR–Chip generated a significant enhancement ( $P=0.0002$ ) in signal output after exposure to 900 ng of its target genomic material relative to control samples lacking the target sequence. Figure 5c indicates the sensitivity of CRISPR–Chip for the detection of HEK-BFP, and Fig. 5d shows real-time monitoring of the *I* response with varying concentrations of HEK-BFP. These results indicate a limit of detection (LOD) of 2.3 fM. In addition, the real-time monitoring of the *I* response indicates that after CRISPR–Chip incubation with genomic samples, the signal reached its saturation within 5 min, showing that this incubation time was sufficient, before rinsing the sensor to remove unbound genomic material, to obtain the final *I* response. Therefore, the total analysis time required for CRISPR–Chip (including sample incubation and the rinsing step) can be estimated as 15 min.

We further examined the dRNP-BFP-functionalized CRISPR–Chip’s ability to specifically bind to its target sequence contained within 900 ng HEK-BFP in the presence of varying concentrations (0–1,800 ng) of the non-target HEK genomic DNA (Fig. 5e). Figure 5f shows the real-time data obtained during this experiment. This result demonstrates that CRISPR–Chip’s *I* response variation in the presence of increasing concentrations of the contaminant DNA was not significant. Figure 5g,h shows a direct comparison between the CRISPR–Chip

*I* response after incubation with 900 ng of HEK-BFP in the presence and absence of 900 ng of HEK genomic contaminant, showing non-significant variation in the *I* response ( $P > 0.05$ ). Figure 5i indicates that PCR yielded a similarly non-significant response to the presence and absence of HEK genomic contaminant ( $P > 0.05$ ).

### **CRISPR–Chip clinical utility for the detection of two mutations within the non-amplified dystrophin gene**

To further validate CRISPR–Chip’s utility for clinical applications, we analysed its ability of to detect Duchenne muscular dystrophy (DMD)-associated mutations. We selected DMD detection as the first clinical model for CRISPR–Chip application due to recent advancement in gene editing technologies, such as CRISPR-based therapeutics<sup>36,37</sup>. DMD is caused by an X-linked dystrophin gene mutation, which can occur across all 79 exons with the most frequent being large deletions at exons 2–10 and 45–55 (refs. <sup>38,39</sup>). These mutations result in the expression of dysfunctional dystrophin, which is a vital protein for mature muscle fibres and proper function of muscle stem cells<sup>40</sup>. The absence of this functional protein leads to continuous degeneration of muscle tissue, and orthopaedic and respiratory complications, which can lead to high morbidity and mortality in DMD patients<sup>41</sup>. Current methodologies to detect DMD include DNA amplification to screen for commonly known deletions within the dystrophin gene and combination methods of measuring levels of creatine kinase paired with genetic testing<sup>42,43</sup>. Early and facile diagnosis of DMD-associated mutations in routine clinical practice, before the onset of severe or lethal symptoms, has the potential to improve treatment outcomes, particularly in the age of gene therapy.

CRISPR–Chip’s ability to detect DMD-associated mutations was evaluated using two dRNPs, which targeted exons 3 and 51 of the human dystrophin gene. These exons are commonly deleted in patients with DMD<sup>39</sup>. Figure 6a shows a schematic of the exons of the dystrophin gene, with highlighted CRISPR–Chip target exons and PCR primer targets. For DMD analysis, CRISPR–Chips were functionalized with either dRNPs specific to exon 3 (dRNP-DMD3) or dRNPs specific to exon 51 (dRNP-DMD51). Both CRISPR–Chip constructs were then incubated with 900 ng of tissue-derived genomic material from male DMD patients (Coriell Institute for Medical Research) with an identified mutation in exon 3 or 51 (ref. <sup>44</sup>). Healthy male genomic samples were obtained from the same vendor and validated for the presence of exon 3 and 51 (Supplementary Fig. 14) before being introduced to both CRISPR–Chip constructs. Figure 6b,c shows that dRNP-DMD3- and dRNP-DMD51-functionalized CRISPR–Chips generated significant enhancement ( $P = 0.00059$ ) in signal output after exposure to genomic samples containing the target exons 3 or 51, relative to DMD samples carrying deletions at exon 3 or 51. Additional experiments were performed to define a negative signal threshold. For these experiments, CRISPR–Chip’s response was evaluated in the presence of the highest concentration of genomic material, obtainable via a commercial buccal sampling method (ep*Motion* 5075 VAC; Eppendorf; ~2,800 ng), from patients with an identified mutation in exon 3 or 51 (Fig. 6d). These experiments allowed for the negative signal threshold to be defined (1.73%), enabling the electrical signal output to be translated to a simple positive or negative result (Fig. 6e).



The results from this study have important implications in the context of rapid and facile identification of genetic mutations associated with hereditary diseases, specifically those involving large fragment deletions and insertions, such as Huntington's disease and haemophilia B<sup>45–47</sup>. Figure 6f shows the sensitivity of dRNP-DMD51-functionalized CRISPR–Chip in the presence of DMD genomic sample containing exon 51 (sample A). This result indicates that the minimum quantity of genomic material required for CRISPR–Chip's amplification-free identification of an exon 51 deletion is comparable to the quantity of genomic material obtainable from non-invasive commercial buccal sampling methods (ep*Motion* 5075 VAC (Eppendorf) and the Centra Puregene Buccal Cell Kit (Qiagen)). The LOD of CRISPR–Chip was found to be  $3.3 \text{ ng } \mu\text{l}^{-1}$ . Considering the molecular weight of the human genome ( $1.9 \times 10^{12} \text{ g mol}^{-1}$ ;  $\sim 2.9 \text{ Cb}$ )<sup>48,49</sup>, this LOD translated to  $1.7 \text{ fM}$  genomic material for DMD analysis. This LOD was calculated according to the equation  $\text{LOD} = 3 s_b/m$  (refs. <sup>50,51</sup>), where  $s_b$  is the standard deviation of the  $I$  response of the negative control ( $2.8 \mu\text{g}$  of DMD sample A) and  $m$  is the slope of the DMD calibration curve (Fig. 6f).

All of the experiments in these studies were performed with three different CRISPR–Chips for each sample analysed. In addition, CRISPR–Chip reproducibility parameters were further investigated by measuring the relative standard deviation (RSD) obtained from dRNP-DMD51-functionalized CRISPR–Chips ( $n = 6$ ) after incubation with  $700 \text{ ng}$  of the same genomic DMD sample A. The results, shown in Fig. 6g, indicate an RSD of 10.6%, which shows good reproducibility for DNA analysis<sup>52</sup>. When performing recovery measurements, an average yield of above 92% was observed (see Supplementary Table 4), showing that CRISPR–Chip is reliable for quantitative analysis of genomic samples<sup>53,54</sup>.

## Discussion

The discovery of Cas and the development of associated technologies has inspired numerous advancements in the field of gene therapy, due to the capacity of the CRISPR–Cas enzymatic system to perform specific targeting, deletions and insertion *in vivo*<sup>55,56</sup>, but these proteins have yet to inspire the same fandom for gene detection applications. We have utilized the catalytically deactivated CRISPR–Cas9 complex as the capture mechanism in this gFET biosensor for rapid identification and quantification of target DNA sequences. gFET biosensors are very attractive for biosensing applications due to their high sensitivity and capability for label-free digital biomolecule detection<sup>31,57</sup>. In particular, CRISPR–Chip utilizes a liquid-gate gFET and a sweeping gate voltage that can mitigate the limitations associated with charge screening effects and reduced sensitivity of the graphene biosensor to the binding events occurring beyond the Debye length<sup>24–26</sup>. The RNA-guided dCas9 complex immobilized on the surface of the graphene within in the CRISPR–Chip gFET construct can specifically bind, enrich and detect the target DNA without the need for reagents and bulky instruments.

The clinical utility of the this first-generation CRISPR–Chip was evaluated for the detection of genetic mutations indicative of DMD. CRISPR–Chip was able to specifically detect the deletion of two target sequences in DMD patients without any pre-amplification. Although CRISPR–Chips were designed to detect only two common DMD exon deletions, these studies indicate that the targeting capacity of CRISPR–Chip can be expanded for multiplex

gene analysis by simply modifying the unique 20-nucleotide sequence at the 5' end of the sgRNA molecule within the dRNP construct. Within the context of DMD, each exon in the dystrophin gene could be targeted to detect disease-causative exon deletions. This proof-of-concept evaluation of CRISPR–Chip also indicated a LOD of 1.7 fM in DMD analysis without amplification. These studies show that CRISPR–Chip may bypass the need for sequence amplification for hereditary disease analysis as the genomic material required for CRISPR–Chip analysis is obtainable via commercially available buccal swab methods<sup>58</sup>. The CRISPR–Chip LOD was lower than for previously reported amplification-free technologies for the detection of target sequences contained within the whole genome<sup>6,59,60</sup>. Although a method based on plasmon resonance imaging with higher sensitivity has been reported<sup>5</sup>, it requires fragmentation of genomic DNA samples via sonication, multiple DNA probes and bulky optical equipment for sequence-specific detection. A direct comparison between CRISPR–Chip and previously reported technologies is reported in Supplementary Table 2. As shown, compared with the alternative techniques for amplification-free genomic analysis, such as gold nanoparticle microarrays and surface plasmon imaging<sup>5</sup>, CRISPR–Chip offers several advantages in a point-of-care context. CRISPR–Chip sample analysis is a three-step process (calibration, incubation and rinsing) that requires only a portable digital reader and reaction buffer, whereas other reported multi-step assay methodologies require multiple reagents and equipment<sup>5,6,59–61</sup>. CRISPR–Chip does not require genomic sample fragmentation, which is commonly achieved by sonication<sup>5,6</sup>; however, similar to other assay methodologies, it does require purification of the genomic sample. Rapid and portable DNA purification methods have been widely reported<sup>62,63</sup>, suggesting that their upstream integration could yield a fully integrated whole genomic digital diagnostic that is more amenable to the point of care.

CRISPR–Chip sensitivity comes from the ability of the anchored dCas9 enzymes to rapidly scan the genome for its target sequence. This sensitivity could be further enhanced by optimizing the density of anchored dCas9 enzymes on the graphene surface. In addition, optimizing the graphene channel geometry and gFET operation parameters, such as voltage and frequency, could also enhance CRISPR–Chip sensitivity<sup>64</sup>. Furthermore, the addition of charged planar molecules, such as methylene blue, after the final rinsing step can enhance the CRISPR–Chip response at lower target concentrations<sup>65</sup>. An example of CRISPR–Chip signal enhancement utilizing methylene blue at a low concentration of the target DNA is shown in Supplementary Fig. 13. Other amplification methodologies such as RPA, used in other CRISPR-based diagnostics technologies, could be utilized to increase the target sequence copy number before CRISPR–Chip analysis<sup>11,66</sup>. This has the potential to expand the utility of CRISPR–Chip for the detection of infectious diseases, which often present low copy numbers in vivo. CRISPR–Chip could also be functionalized with other Cas proteins, such as Cas13a, for the detection of RNA-based target sequences<sup>11</sup>, further expanding its diagnostic potential.

Lastly, CRISPR–Chip could not only improve access to genetic information with facile and early disease risk prediction and diagnosis, but it could also provide information about the affinity of sgRNA to various Cas enzymes via the observation of association/dissociation kinetics (Supplementary Fig. 12). For example, CRISPR–Chip could be utilized as an optimization tool for validation and CRISPR complex formation efficacy prediction in



various environments, designed to mimic a desired cellular target<sup>67</sup>. An example of real-time information that can be obtained by CRISPR–Chip is presented in Supplementary Fig. 11. With the fast-expanding development of a broad range of CRISPR enzymes, such as newly developed MAD7 enzymes<sup>68,69</sup>, CRISPR–Chip’s utility as an affinity analysis tool is pertinent.

CRISPR–Chip is a promising tool, constructed from two propitious technologies—a graphene-based biosensor and CRISPR technology—and it has the potential to extend the boundaries of digital genomics. Future work invites more studies to enhance the capability of CRISPR–Chip to detect single nucleotide polymorphisms, which could significantly broaden its future clinical application.

## Methods

### Graphene-based FET sensor fabrication

Graphene chips were obtained from a commercial foundry (Cardea Bio). The chips were fabricated in several stages using conventional microelectromechanical systems processing<sup>27</sup>. The gFET was constructed according to published literature<sup>27,70</sup>. Briefly, Ti/Pt source, drain and reference electrodes with corresponding bond pads were patterned on 6’ silicon wafers using a lift-off processing technique. Wafers were then cleaned by piranha etching to remove all potential organic residues that could act as dopants of the final graphene devices. High-quality graphene films grown on a copper foil substrate were spin coated with a poly methyl methacrylate support layer, then delaminated from the copper foil substrate by bubbling transfer<sup>71</sup>. The graphene films were then deposited on top of the electrode-patterned wafers and thoroughly cleaned with acetone and isopropanol. Graphene sheets were then patterned to form defined channels between the source and drain electrodes using plasma-enhanced chemical vapour deposition to deposit a silicon oxide layer over the entire wafer, and reactive ion etching to etch the graphene transistors<sup>64</sup>. Two-terminal electrical resistance characterization of the devices indicated a yield of >98% of functional graphene devices. The patterned graphene wafers were then diced into 9 mm × 9 mm dice and each chip was attached to a custom-printed circuit board package using epoxy. The circuit board was then encapsulated in epoxy, leaving an open cavity over the exposed graphene transistors for biological sample placement.

### Measurement method

The CRISPR–Chip response is measured continuously utilizing a commercial reader (Agile R100; Nanomedical Diagnostics) and reported based on equation (1). For this measurement, the liquid-gate voltage was swept between ±100 mV at a slow speed of 0.3 Hz, while  $V_{ds}$  (the voltage applied across the drain and source electrodes) was held at 50 mV. The gate sweeping frequency mitigates the charge screening effect due to the non-specific adsorption of ions on the surface of the graphene<sup>72,73</sup>.

### Single-guide RNA design and evaluation

For *bfp* genomic analysis via CRISPR–Chip, the *bfp*-targeting sgRNA was designed and validated according to published literature<sup>36</sup> (see Supplementary Fig. 7). The *bfp*-specific

sgRNA targeted the sequence GCTGAAGCACTGCACGCCATGG. For DMD analysis via CRISPR–Chip, two sgRNAs were designed and validated to target exons 3 and 51 of the human dystrophin gene by Thermo Fisher Scientific (TrueGuide and SS Oligo Design) and were ordered from Synthego and Invitrogen. The exon 3-targeting sgRNA (sgRNA-DMD3) targeted the sequence CTCTTCAGTGACCTACAGGA, whereas the exon 51-targeting sgRNA (sgRNA-DMD51) targeted the sequence CTTGGACAGAACTTACCGAC (Figs. 6b,c).

### Genomic samples for CRISPR–Chip analysis

For *bfp* detection via CRISPR–Chip, target HEK-BFP and non-target HEK genomic materials lacking the *bfp* sequence were utilized. Briefly, HEK-BFP DNA was extracted from *bfp*-transduced HEK293T cells (PureLink Genomic DNA Mini Kit; Thermo Fisher Scientific) and purified (QIAquick PCR Purification Kit; Qiagen) according to the manufacturer's instructions and published protocol<sup>36</sup>. For analysis of DMD-associated mutations via CRISPR–Chip, human genomic samples from both healthy male and DMD male patients were purchased with certificate of analysis from the Coriell Institute for Medical Research. DMD samples presented in this study carried previously identified large-scale fragment deletions: A (NA07691)<sup>44</sup>, B (NA03780)<sup>44</sup>, C (NA03782)<sup>44</sup>, D (NA04100)<sup>44</sup>, E (NA05126)<sup>44</sup> and F (NA04364)<sup>44</sup>. Healthy samples—H1 (NA22264), H2 (NA22807) and H3 (NA03798)—were also validated for the presence of target exons (see Supplementary Fig. 14). The concentration of genomic material was routinely measured before incubation with CRISPR–Chip using Nanodrop (Infinite M200 NanoQuant; Tecan).

### CRISPR–Chip molecular linker functionalization and activation

The CRISPR–Chip graphene biosensor, fabricated as described above, was cleaned twice with acetone and once with deionized water. Subsequently, it was functionalized by first incubating PBA (5 mM; 15  $\mu$ l; Sigma–Aldrich) in dimethylformamide onto the graphene surface for 2 h at room temperature or overnight at 4 °C. The surface of the graphene sensor was then rinsed twice with dimethylformamide and once with deionized water and allowed to dry completely. The PBA was then activated using a 1:1 volume ratio of *N*-(3-dimethylaminopropyl)-*N'*-ethylcarbodiimide hydrochloride (4 mM) and *N*-hydroxysuccinimide (11 mM) (Sigma–Aldrich) in 50 mM of 2-(*N*-morpholino)ethanesulfonic acid (pH 6) for 5 min at room temperature according to published studies<sup>74,75</sup> before incubation with dCas9.

### dCas9-sgRNA (dRNP) immobilization on the graphene surface

After PBA linker immobilization and activation on the surface of the graphene, 900 ng (30  $\mu$ l in 2 mM MgCl<sub>2</sub> of dCas9 (University of California, Berkeley MacroLab) was incubated for 15 min at 37 °C on the surface of the graphene. The CRISPR–Chip *I* response was monitored continuously. Unreacted PBA molecules on the graphene surface were then blocked using amino-PEG5-alcohol (1 mM, 10 min at 37 °C) and ethanolamine hydrochloride (1 M, 10 min at 37 °C) (Sigma–Aldrich). After blocking, the graphene surface was washed with 2 mM MgCl<sub>2</sub> solution and incubated until the *I* response readings stabilized. To form the dRNP complex, 900 ng (30  $\mu$ l in 2 mM MgCl<sub>2</sub> of sgRNA specific to

the target sequence was introduced onto the graphene surface and incubated for 10 min at 37 °C to form dRNPs. sgRNA samples were thermally treated to remove the dimer structure before incubation with the CRISPR–Chip76. The CRISPR–Chip was then washed with 2 mM MgCl<sub>2</sub> for 5 min to remove any unbound sgRNA. This final step resulted in full dRNP formation on the graphene surface and a functional CRISPR–Chip.

### CRISPR–Chip evaluation of *bfp* PCR products

dRNP-BFP-functionalized CRISPR–Chips were incubated with 1,800 ng of *bfp* PCR product (30 µl, 2 mM MgCl<sub>2</sub> for 30 min at 37 °C (see the section ‘Genomic *bfp* PCR amplification’). As a negative control, the dRNP-Scram-functionalized CRISPR–Chip was incubated with 1,800 ng of *bfp* PCR product (30 µl, 2 mM MgCl<sub>2</sub> for 30 min at 37 °C. The sensor was rinsed (2 mM MgCl<sub>2</sub>, 30 µl) for 15 min at 37 °C after incubation with the dsDNA sample. The *I* response was continuously monitored.

### Affinity of dRNP-BFP-functionalized MBs to HEK-BFP

MBs (1 µm; Dynabeads MyOne Carboxylic Acid; Invitrogen) were functionalized with dRNP-BFP to evaluate the dRNP-BFP complex’s affinity to target sequences contained within whole genomic samples. Briefly, carboxylated MBs were activated using *N*-(3-dimethylaminopropyl)-*N*’-ethylcarbodiimide hydrochloride (26 mM in 10 mM potassium phosphate, 0.15 M NaCl) and sulfo-*N*-hydroxysuccinimide (23 mM in 10 mM potassium phosphate, 0.15 M NaCl) according to the published protocol<sup>77</sup>. Activated MBs were promptly coupled with dCas9 (33.3 ng µl<sup>-1</sup> in 10 mM potassium phosphate, 0.15 M NaCl) for 3 h. After dCas9 coupling, MBs were blocked for 30 min at room temperature using glycine (1.0 M). The complete MB-dRNP-BFP complex was formed by incubating MBs coupled with dCas9 (3.3 µg µl<sup>-1</sup> in 2 mM MgCl<sub>2</sub>) with sgRNA (30 ng µl<sup>-1</sup> in 2 mM MgCl<sub>2</sub>) specific to *bfp* for 30 min at 37 °C. This fully functional MB-dRNP-BFP complex was then incubated with 20 ng of HEK-BFP (30 µl in 2 mM MgCl<sub>2</sub>). HEK-BFP samples were incubated with MB-dRNP-BFP (3.3 µg µl<sup>-1</sup>) for 1 h at 37 °C. For control experiments, HEK DNA was also incubated with the MB-dRNP-BFP complex. After magnetic separation, the supernatant was eluted and evaluated using gel electrophoresis (100 V for 1.5 h). Example gel images are presented in Supplementary Fig. 10. The intensities of the bands were quantified with ImageJ (National Institutes of Health).

### CRISPR–Chip evaluation for the detection of HEK-BFP

The dRNP-BFP-functionalized CRISPR–Chips were calibrated with 2 mM MgCl<sub>2</sub> for 5 min at 37 °C and subsequently incubated with varying concentrations (300–1,200 ng) of HEK-BFP (30 µl in 2 mM MgCl<sub>2</sub> for 30 min at 37 °C. For the control experiments, HEK DNA was incubated with dRNP-BFP-functionalized CRISPR–Chips. For all experiments, the sensor was rinsed (2 mM MgCl<sub>2</sub>, 30 µl) for 20 min at 37 °C after incubation with the genomic sample.

### CRISPR–Chip detection of HEK-BFP in the presence of HEK DNA contamination

The dRNP-BFP-functionalized CRISPR–Chips were calibrated with 2 mM MgCl<sub>2</sub> for 5 min at 37 °C and subsequently incubated with 900 ng HEK-BFP DNA mixed with varied

concentrations (0–1,800 ng) of HEK DNA (30  $\mu$ l in 2 mM MgCl<sub>2</sub>). The CRISPR–Chip response was continuously monitored for 30 min at 37 °C. CRISPR–Chips were then rinsed (2 mM MgCl<sub>2</sub>, 30  $\mu$ l) for 20 min at 37 °C after incubation with the genomic sample.

### Genomic *bfp* PCR amplification

*bfp* was amplified from 900 ng HEK-BFP via PCR according to the published literature and manufacturer's protocols. The forward and reverse primer sequences were TGTCCGGCGAGGGCGAGGGCGAT and CGTCCTTGAAGAAGATGGTGCGC, respectively<sup>36</sup>. The following thermal cycler PCR protocol was used with a Phusion High-Fidelity PCR Kit (Thermo Fisher Scientific): (1) 98 °C for 30 s; (2) 98 °C for 10 s; (3) 63.5 °C for 10 s; (4) 72 °C for 10 s; (5) 72 °C for 2 min; (6) hold at 4 °C; and (7) repeat steps (2)–(4) 30 $\times$ . For PCR in the presence of HEK DNA contamination, *bfp* was amplified from a mixture of 900 ng of HEK-BFP and 900 ng of HEK DNA. As a negative control, PCR was also performed on 900 ng of HEK DNA.

### CRISPR–Chip evaluation for the detection of DMD-associated large fragment deletions

The dRNP-DMD3- and dRNP-DMD51-functionalized CRISPR–Chips were calibrated with 2 mM MgCl<sub>2</sub> for 5 min at 37 °C and subsequently incubated with 900 ng (30  $\mu$ l, 2 mM MgCl<sub>2</sub>) genomic clinical sample. A total of nine samples were analysed (see 'Genomic samples for CRISPR–Chip analysis'). dRNP-DMD3- and dRNP-DMD51-functionalized CRISPR–Chip *I* responses were continuously monitored for 25 min at 37 °C in the presence of each genomic clinical sample. CRISPR–Chips were then rinsed (2 mM MgCl<sub>2</sub>, 30  $\mu$ l) for 15 min at 37 °C after incubation with the genomic sample. For sensitivity evaluation, dRNP-DMD51-functionalized CRISPR–Chips were calibrated with 2 mM MgCl<sub>2</sub> for 5 min at 37 °C and subsequently incubated with varied concentrations of sample A (400–1,500 ng) (30  $\mu$ l, 2 mM MgCl<sub>2</sub>). *I* responses were continuously monitored for 25 min at 37 °C. CRISPR–Chips were then rinsed (2 mM MgCl<sub>2</sub>, 30  $\mu$ l) for 15 min at 37 °C after incubation with sample A.

### Definition of the DMD-negative CRISPR–Chip response threshold

The dRNP-DMD3- and dRNP-DMD51-functionalized CRISPR–Chips were calibrated with 2 mM MgCl<sub>2</sub> for 5 min at 37 °C and subsequently incubated with 2.8  $\mu$ g (30  $\mu$ l, 2 mM MgCl<sub>2</sub>) genomic clinical sample, which was the highest reported yield for obtaining genomic material from a single buccal swab (*epMotion* 5075 VAC; Eppendorf). The dRNP-DMD3-functionalized CRISPR–Chip was incubated with sample B (NA03780) and the dRNP-DMD51-functionalized CRISPR–Chip was incubated with sample E (NA05126) for 25 min. CRISPR–Chips were then rinsed (2 mM MgCl<sub>2</sub>, 30  $\mu$ l) for 15 min at 37 °C after incubation with the genomic sample.

### Chip reproducibility

The reproducibility of CRISPR–Chip was evaluated by measuring the RSD of *I* responses obtained from six dRNP-DMD51-functionalized CRISPR–Chips. The dRNP-DMD51-functionalized CRISPR–Chips were calibrated with 2 mM MgCl<sub>2</sub> for 5 min at 37 °C and subsequently incubated with 700 ng genomic clinical sample A (30  $\mu$ l, 2 mM MgCl<sub>2</sub>) for 25

min at 37 °C (for the vendor catalogue number, see the Supplementary Information). CRISPR–Chips were then rinsed (2 mM MgCl<sub>2</sub>, 30 µl) for 15 min at 37 °C after incubation with the genomic sample, and *I* responses were analysed.

### Reporting summary

Further information on research design is available in the Nature Research Reporting Summary linked to this article.

### Data availability

The authors declare that all data supporting the findings in this study are available within the paper and its Supplementary Information files.

### Supplementary Material

Refer to Web version on PubMed Central for supplementary material.

### Acknowledgements

We acknowledge Cardea Bio for our use of their Agile R100 reader technology. We thank J. Corn (University of California, Berkeley) for providing us with the HEK-BFP cells.

This work was primarily supported by Keck Start-up funding to the Aran Lab, by an Open Philanthropy Research Gift and by the Rogers Family Foundation to I.C.

### References

1. Yuen RKC et al. Whole genome sequencing resource identifies 18 new candidate genes for autism spectrum disorder. *Nat. Neurosci* 20, 602–611 (2017). [PubMed: 28263302]
2. Iyer G et al. Genome sequencing identifies a basis for everolimus sensitivity. *Science* 338, 221 (2012). [PubMed: 22923433]
3. Waddell N et al. Whole genomes redefine the mutational landscape of pancreatic cancer. *Nature* 518, 495–501 (2015). [PubMed: 25719666]
4. Wu D et al. A label-free colorimetric isothermal cascade amplification for the detection of disease-related nucleic acids based on double-hairpin molecular beacon. *Anal. Chim. Acta* 957, 55–62 (2017). [PubMed: 28107834]
5. Ermini ML, Mariani S, Scarano S & Minunni M Direct detection of genomic DNA by surface plasmon resonance imaging: an optimized approach. *Biosens. Bioelectron* 40, 193–199 (2013). [PubMed: 22857906]
6. Bao YP et al. SNP identification in unamplified human genomic DNA with gold nanoparticle probes. *Nucleic Acids Res.* 33, e15–e15 (2005). [PubMed: 15659576]
7. Bartlett JMS & Stirling D in *PCR Protocols* (eds Bartlett JMS & Stirling D) 3–6 (Humana Press, 2003).
8. Cao L et al. Advances in digital polymerase chain reaction (dPCR) and its emerging biomedical applications. *Biosens. Bioelectron.* 90, 459–474 (2017). [PubMed: 27818047]
9. Furlan I, Domljanovic I, Uhd J & Astakhova K Improving design of synthetic oligonucleotide probes by fluorescence melting assay. *ChemBioChem* 20, 587–594 (2019). [PubMed: 30211970]
10. Busse N et al. Detection and localization of viral infection in the pancreas of patients with type 1 diabetes using short fluorescently-labelled oligonucleotide probes. *Oncotarget* 8, 12620–12636 (2017). [PubMed: 28147344]
11. Gootenberg JS et al. Nucleic acid detection with CRISPR–Cas13a/C2c2. *Science* 365, 438–442 (2017).

12. Li S-Y et al. CRISPR–Cas12a-assisted nucleic acid detection. *Cell Discov.* 4, 20 (2018). [PubMed: 29707234]
13. Pardee K et al. Rapid, low-cost detection of Zika virus using programmable biomolecular components. *Cell* 165, 1255–1266 (2016). [PubMed: 27160350]
14. Chen JS et al. CRISPR–Cas12a target binding unleashes indiscriminate single-stranded DNase activity. *Science* 360, 436–439 (2018). [PubMed: 29449511]
15. Jinek M et al. A programmable dual-RNA-guided DNA endonuclease in adaptive bacterial immunity. *Science* 337, 816–821 (2012). [PubMed: 22745249]
16. Zheng C et al. Fabrication of ultrasensitive field-effect transistor DNA biosensors by a directional transfer technique based on CVD-grown graphene. *aCs Appl. Mater. Interfaces* 7, 16953–16959 (2015). [PubMed: 26203889]
17. Reddy D, Register LF, Carpenter GD & Banerjee SK Graphene field-effect transistors. *J. Phys. Appl. Phys* 44, 313001 (2011).
18. Mekler V, Minakhin L & Severinov K Mechanism of duplex DNA destabilization by RNA-guided Cas9 nuclease during target interrogation. *Proc. Natl Acad. Sci. USA* 114, 5443–5448 (2017). [PubMed: 28484024]
19. Sternberg SH, Redding S, Jinek M, Greene EC & Doudna JA DNA interrogation by the CRISPR RNA-guided endonuclease Cas9. *Nature* 507, 62–67 (2014). [PubMed: 24476820]
20. Lin S, Staahl BT, Alla RK & Doudna JA Enhanced homology-directed human genome engineering by controlled timing of CRISPR/Cas9 delivery. *eLife* 3, e04766 (2014). [PubMed: 25497837]
21. Georgakilas V et al. Noncovalent functionalization of graphene and graphene oxide for energy materials, biosensing, catalytic, and biomedical applications. *Chem. Rev* 116, 5464–5519 (2016). [PubMed: 27033639]
22. Ohshima H & Ohki S Donnan potential and surface potential of a charged membrane. *Biophys. J* 47, 673–678 (1985). [PubMed: 4016187]
23. Bergveld P A critical evaluation of direct electrical protein detection methods. *Biosens. Bioelectron.* 6, 55–72 (1991). [PubMed: 2049171]
24. Schasfoort RBM, Bergveld P, Kooyman RPH & Greve J Possibilities and limitations of direct detection of protein charges by means of an immunological field-effect transistor. *Anal. Chim. Acta* 238, 323–329 (1990).
25. Kaisti M Detection principles of biological and chemical FET sensors. *Biosens. Bioelectron* 98, 437–448 (2017). [PubMed: 28711826]
26. Palazzo G et al. Detection beyond Debye’s length with an electrolyte-gated organic field-effect transistor. *Adv. Mater.* 27, 911–916 (2015). [PubMed: 25376989]
27. Lerner MB et al. Large scale commercial fabrication of high quality graphene-based assays for biomolecule detection. *Sens. Actuators B Chem* 239, 1261–1267 (2017).
28. Lepvrier E, Doigneaux C, Moullintraffort L, Nazabal A & Garnier C Optimized protocol for protein macrocomplexes stabilization using the EDC, 1-ethyl-3-(3-(dimethylamino)propyl)carbodiimide, zero-length cross-linker. *Anal. Chem* 86, 10524–10530 (2014). [PubMed: 25268573]
29. Johnsson B, Lofas S & Lindquist G Immobilization of proteins to a carboxymethyl-dextran-modified gold surface for biospecific interaction analysis in surface plasmon resonance sensors. *Anal. Biochem* 198, 268–277 (1991). [PubMed: 1724720]
30. Gao N et al. Specific detection of biomolecules in physiological solutions using graphene transistor biosensors. *Proc. Natl Acad. Sci. USA* 113, 14633–14638 (2016). [PubMed: 27930344]
31. Afsahi S et al. Novel graphene-based biosensor for early detection of Zika virus infection. *Biosens. Bioelectron* 100, 85–88 (2018). [PubMed: 28865242]
32. Liu B et al. Parts-per-million of polyethylene glycol as a non-interfering blocking agent for homogeneous biosensor development. *Anal. Chem* 85, 10045–10050 (2013). [PubMed: 24067133]
33. Glaser A, McColl B & Vadolas J GFP to BFP conversion: a versatile assay for the quantification of CRISPR/Cas9-mediated genome editing. *Mol. Ther. Nucleic Acids* 5, e334 (2016). [PubMed: 27404719]



34. Richardson CD et al. CRISPR–Cas9 genome editing in human cells occurs via the Fanconi anemia pathway. *Nat. Genet* 50, 1132–1139 (2018). [PubMed: 30054595]
35. Deboer TR, Wauford N, Chung J-Y, Torres Perez MS & Murthy N A cleavage-responsive stem-loop hairpin for assaying guide RNA activity. *ACS Chem Biol.* 13, 461–466 (2018). [PubMed: 29381046]
36. Lee K et al. Nanoparticle delivery of Cas9 ribonucleoprotein and donor DNA in vivo induces homology-directed DNA repair. *Nat. Biomed. Eng* 1, 889–901 (2017). [PubMed: 29805845]
37. Amosii L et al. Gene editing restores dystrophin expression in a canine model of Duchenne muscular dystrophy. *Science* 362, 86–91 (2018). [PubMed: 30166439]
38. Den Dunnen JT et al. Topography of the Duchenne muscular dystrophy (DMD) gene: FIGE and cDNA analysis of 194 cases reveals 115 deletions and 13 duplications. *Am. J. Hum. Genet* 45, 835–847 (1989). [PubMed: 2573997]
39. Aartsma-Rus A, Ginjaar IB & Bushby K The importance of genetic diagnosis for Duchenne muscular dystrophy. *J. Med. Genet* 53, 145–151 (2016). [PubMed: 26754139]
40. Dumont NA et al. Dystrophin expression in muscle stem cells regulates their polarity and asymmetric division. *Nat. Med* 21, 1455–1463 (2015). [PubMed: 26569381]
41. Allen DG, Whitehead NP & Froehner SC Absence of dystrophin disrupts skeletal muscle signaling: roles of Ca<sup>2+</sup>, reactive oxygen species, and nitric oxide in the development of muscular dystrophy. *Physiol. Rev* 96, 253–305 (2016). [PubMed: 26676145]
42. Mendell JR et al. Evidence-based path to newborn screening for Duchenne muscular dystrophy. *Ann. Neurol* 71, 304–313 (2012). [PubMed: 22451200]
43. Chamberlain JS, Gibbs RA, Rainer JE, Nguyen PN & Thomas C Deletion screening of the Duchenne muscular dystrophy locus via multiplex DNA amplification. *Nucleic Acids Res.* 16, 11141–11156 (1988). [PubMed: 3205741]
44. Tang Z et al. A dynamic database of microarray-characterized cell lines with various cytogenetic and genomic backgrounds. *G3 (Bethesda)* 3, 1143–1149 (2013). [PubMed: 23665875]
45. Myers RH Huntington’s disease genetics. *NeuroRx* 1, 255–262 (2004). [PubMed: 15717026]
46. Koeberl DD et al. Mutations causing hemophilia B: direct estimate of the underlying rates of spontaneous germ-line transitions, transversions, and deletions in a human gene. *Am. J. Hum. Genet* 47, 202–217 (1990). [PubMed: 2198809]
47. Giannelli F et al. Gene deletions in patients with haemophilia B and anti-factor IX antibodies. *Nature* 303, 181–182 (1983). [PubMed: 6843667]
48. D’Agata R et al. Direct detection of point mutations in nonamplified human genomic DNA. *Anal. Chem.* 83, 8711–8717 (2011). [PubMed: 21978174]
49. International Human Genome Sequencing Consortium. Finishing the euchromatic sequence of the human genome. *Nature* 431, 931–945 (2004). [PubMed: 15496913]
50. Long GL & Winefordner JD Limit of detection. A closer look at the IUPAC definition. *Anal. Chem* 55, 712A–724A (1983).
51. Muhammad A et al. A screen printed carbon electrode modified with carbon nanotubes and gold nanoparticles as a sensitive electrochemical sensor for determination of thiamphenicol residue in milk. *RSC Adv.* 8, 2714–2722 (2018).
52. Wu W et al. Low-cost, disposable, flexible and highly reproducible screen printed SERS substrates for the detection of various chemicals. *Sci. Rep* 5, 10208 (2015). [PubMed: 25974125]
53. Shams N et al. A promising electrochemical sensor based on Au nanoparticles decorated reduced graphene oxide for selective detection of herbicide diuron in natural waters. *J. Appl. Electrochem* 46, 655–666 (2016).
54. Shams N et al. Electrochemical sensor based on gold nanoparticles/ethylenediamine-reduced graphene oxide for trace determination of fenitrothion in water. *RSC Adv.* 6, 89430–89439 (2016).
55. Hsu PD, Lander ES & Zhang F Development and applications of CRISPR–Cas9 for genome engineering. *Cell* 157, 1262–1278 (2014). [PubMed: 24906146]
56. Adli M The CRISPR tool kit for genome editing and beyond. *Nat. Commun.* 9, 1911 (2018). [PubMed: 29765029]

57. Huang Y et al. Nanoelectronic biosensors based on CVD grown graphene. *Nanoscale* 2, 1485–1488 (2010). [PubMed: 20820739]
58. Boughanem H & Macias-Gonzalez M High-Throughput Isolation of Genomic DNA From Buccal Swab on the Eppendorf epMotion® 5075 VAC (Eppendorf, 2016).
59. Storhoff JJ et al. Gold nanoparticle-based detection of genomic DNA targets on microarrays using a novel optical detection system. *Biosens. Bioelectron* 19, 875–883 (2004). [PubMed: 15128107]
60. Jung YL, Jung C, Park JH, Kim MI & Park HG Direct detection of unamplified genomic DNA based on photo-induced silver ion reduction by DNA molecules. *Chem. Commun* 49, 2350–2352 (2013).
61. Storhoff JJ, Lucas AD, Garimella V, Bao YP & Müller UR Homogeneous detection of unamplified genomic DNA sequences based on colorimetric scatter of gold nanoparticle probes. *Nat. Biotechnol* 22, 883–887 (2004). [PubMed: 15170215]
62. Kalyanasundaram D et al. Rapid extraction and preservation of genomic DNA from human samples. *Anal. Bioanal. Chem.* 405, 1977–1983 (2013). [PubMed: 23307121]
63. Rodriguez NM, Wong WS, Liu L, Dewar R & Klapperich CM A fully integrated paperfluidic molecular diagnostic chip for the extraction, amplification, and detection of nucleic acids from clinical samples. *Lab Chip* 16, 753–763 (2016). [PubMed: 26785636]
64. Stine R, Mulvaney SP, Robinson JT, Tamana CR & Sheehan PE Fabrication, optimization, and use of graphene field effect sensors. *Anal. Chem* 85, 509–521 (2013). [PubMed: 23234380]
65. Tuite E & Norden B Sequence-specific interactions of methylene blue with polynucleotides and DNA: a spectroscopic study. *J. Am. Chem. Soc* 116, 7548–7556 (1994).
66. Lau HY et al. Specific and sensitive isothermal electrochemical biosensor for plant pathogen DNA detection with colloidal gold nanoparticles as probes. *Sci. Rep.* 7, 38896 (2017). [PubMed: 28094255]
67. Jiang F & Doudna JA CRISPR–Cas9 structures and mechanisms. *Annu. Rev. Biophys* 46, 505–529 (2017). [PubMed: 28375731]
68. Gill RT, Garst A & Lipscomb TE W Nucleic acid-guided nucleases. US patent 10,011,849 (2018).
69. Gill RT, Garst A & Lipscomb TE W Nucleic acid-guided nucleases. US patent 9,982,279 (2018).
70. Goldsmith BR et al. Digital biosensing by foundry-fabricated graphene sensors. *Sci. Rep* 9, 434 (2019). [PubMed: 30670783]
71. Gao L et al. Repeated growth and bubbling transfer of graphene with millimetre-size single-crystal grains using platinum. *Nat. Commun* 3, 697–699 (2012). [PubMed: 22426218]
72. Kulkarni GS & Zhong Z Detection beyond the Debye screening length in a high-frequency nanoelectronic biosensor. *Nano Lett.* 12, 719–723 (2012). [PubMed: 22214376]
73. Munje RD, Muthukumar S, Selvam AP & Prasad S Flexible nanoporous tunable electrical double layer biosensors for sweat diagnostics. *Sci. Rep* 5, 14586 (2015). [PubMed: 26420511]
74. Wang C, Yan Q, Liu HB, Zhou XH & Xiao SJ Different EDC/NHS activation mechanisms between PAA and PMAA brushes and the following amidation reactions. *Langmuir* 27, 12058–12068 (2011). [PubMed: 21853994]
75. Everaerts F, Torrianni M, Hendriks M & Feijen J Biomechanical properties of carbodiimide crosslinked collagen: influence of the formation of ester crosslinks. *J. Biomed. Mater. Res. A* 85, 547–555 (2008). [PubMed: 17729260]
76. Dang Y et al. Optimizing sgRNA structure to improve CRISPR–Cas9 knockout efficiency. *Genome Biol.* 16, 280 (2015). [PubMed: 26671237]
77. BcMag Carboxy-Terminated Magnetic Beads (Bioclone, 2004).

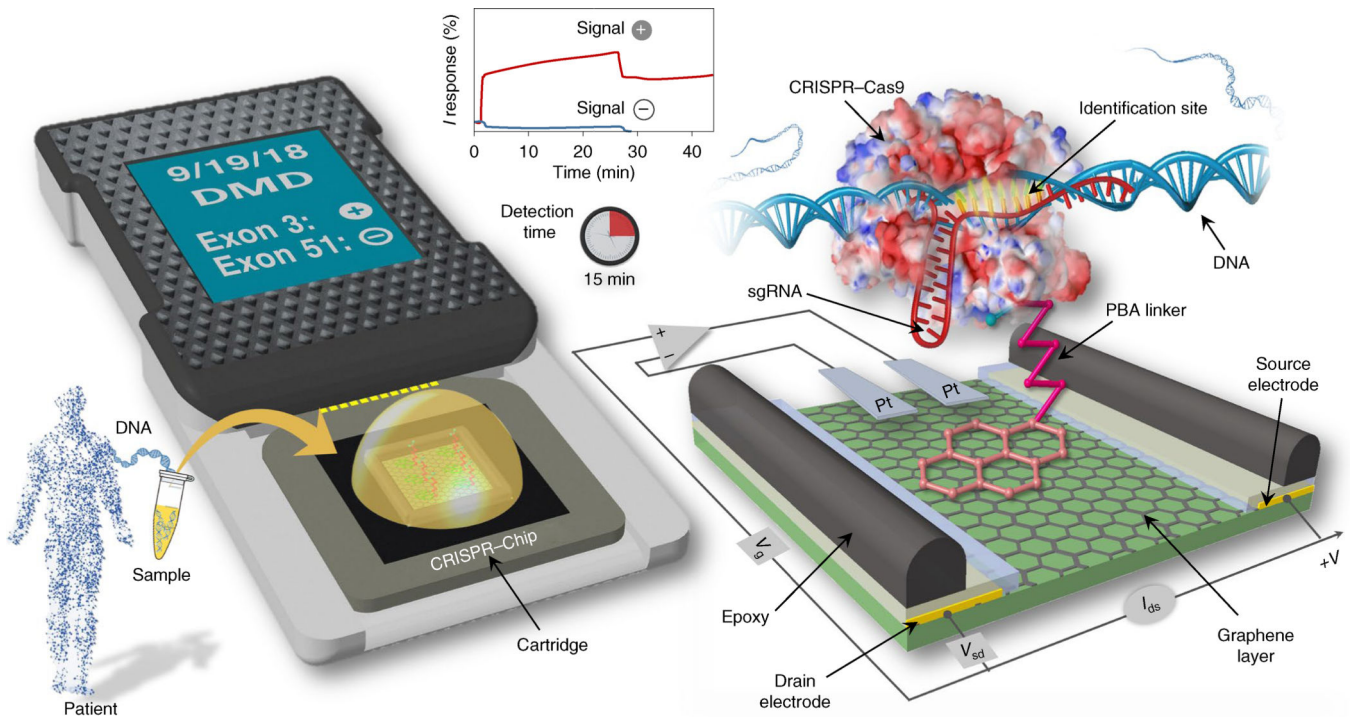


**Fig. 1 | CRISPR-Chip enables gene detection in less than 15 min.**

CRISPR-Chip exploits the gene-targeting capacity of CRISPR-Cas9 and the sensitivity of gFET to enable rapid detection of a gene target from the whole genomic sample without amplification. The dCas9 complexed with a target-specific sgRNA (referred to as dRNP) is immobilized on the surface of the graphene within the gFET construct. The immobilized dRNP scans the whole genomic DNA until it identifies its target sequence (complementary to the 5' end of sgRNA), unzips the double helix and kinetically binds to the DNA target. The selective binding event of the target DNA to the dRNP complex modulates the electrical characteristics of the gFET and results in an electrical signal output within 15 min.

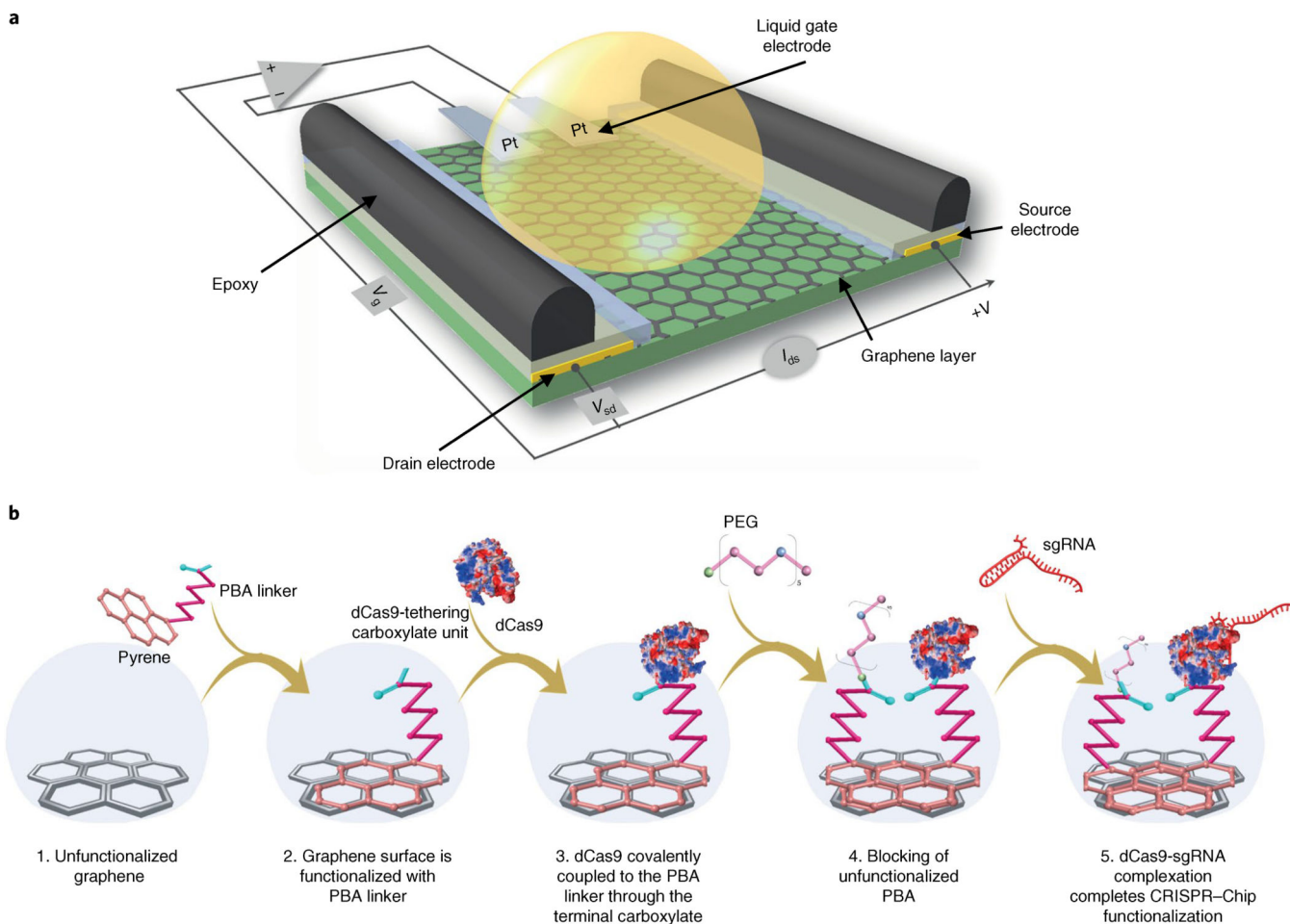


**Fig. 2 | CRISPR-Chip is a liquid-gate field-effect transistor functionalized with CRISPR-dCas9.** **a**, CRISPR-Chip is composed of a three-terminal gFET, which utilizes dRNP-functionalized graphene as a channel between the source and the drain electrodes, with a liquid gate that is in contact with the genomic sample. The binding of the dRNP to its target DNA results in modulation of graphene conductivity and Donnan potential, which results in a change in the electrical characteristics of the transistor. **b**, Schematics of CRISPR-Chip functionalization. The graphene surface of the gFET is first functionalized with a heterofunctional PBA linker comprised of a planar pyrene ring system that electrostatically interacts with the  $\pi$ -system of graphene. A carboxylate group (highlighted in light blue) at the terminal end of the hydrocarbon arm (highlighted in pink) of the PBA linker acts as the dCas9-tethering unit that covalently couples to dCas9, securing the nuclease to the surface of graphene. Any unfunctionalized PBA molecules are blocked with amino-polyethylene glycol 5-alcohol (PEG). Finally, sgRNA complementary to a gene of interest is introduced and complexes with dCas9 tethered to the graphene surface. Complexation of the sgRNA to dCas9 affords the functional gene-targeting dRNP unit and completes CRISPR-Chip functionalization.

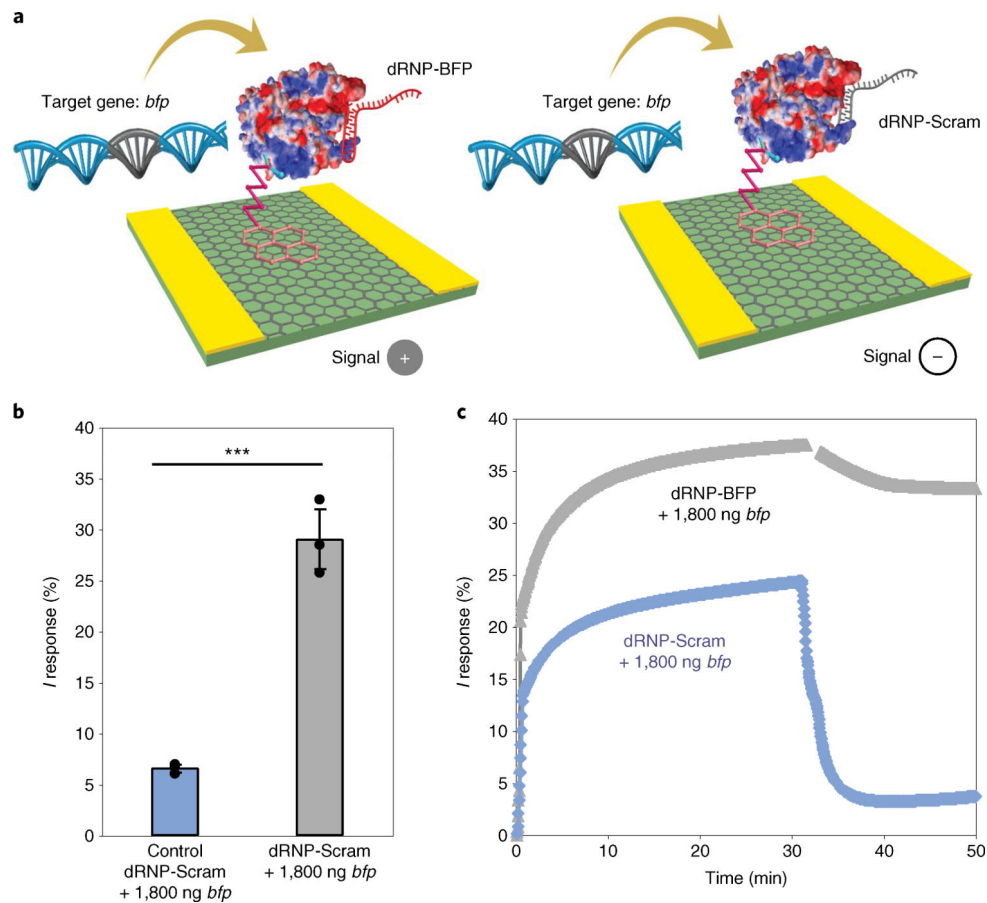


**Fig. 3 |. CRISPR–Chip selectively detects the gene target *bfp*.**

To show selectivity, CRISPR–Chips were functionalized with dRNP-BFP (denoted with the red sgRNA) to target the *bfp* gene and dRNP-Scram (denoted with the grey sgRNA) as a negative control. **a**, *bfp* PCR products were analysed on both the *bfp*-targeting CRISPR–Chip (left) and the Scram-targeting CRISPR–Chip (right). **b**, The *I* response of the *bfp*-targeting CRISPR–Chip in the presence of the *bfp* PCR product was significantly higher ( $***P = 0.0002$ , two-tailed *t*-test,  $n = 3$ ) than that generated by the Scram-targeting CRISPR–Chip. **c**, The dRNP-BFP-functionalized CRISPR–Chip representative real-time *I* response detected its target dsDNA in 2.5 min. Error bars represent s.d.



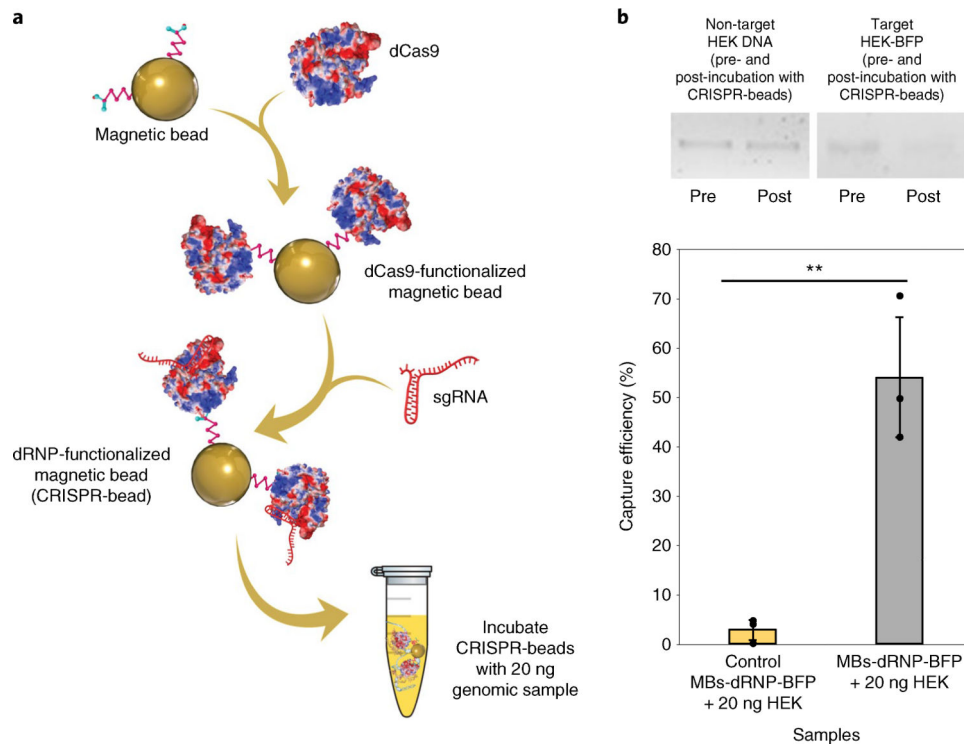


**Fig. 4 | The gene-targeting dRNP unit effectively binds a selective gene locus in genomic DNA.**  
**a**, A CRISPR-functionalized MB was synthesized to evaluate the binding capacity of the dRNP for its target gene contained within whole genomic samples. The CRISPR-functionalized MB was produced by first covalently attaching dCas9 to the MB surface, then incubating with sgRNA-BFP. Finally, genomic material was incubated with the functional CRISPR-beads for 30 min at 37 °C. **b**, The capture efficiency of the BFP-dRNP-functionalized CRISPR-beads was evaluated by gel electrophoresis to determine the amount of non-target HEK genomic material, or target HEK-BFP genomic material that was captured by the beads. The dRNP-BFP was significantly more able to bind and maintain its affinity to its target genomic material extract (HEK-BFP; ~54%) compared with non-target genomic material (\*\* $P = 0.002$ , two-tailed  $t$ -test,  $n = 3$ ). Error bars represent s.d. See Supplementary Fig. 10 for full scans of the gels.



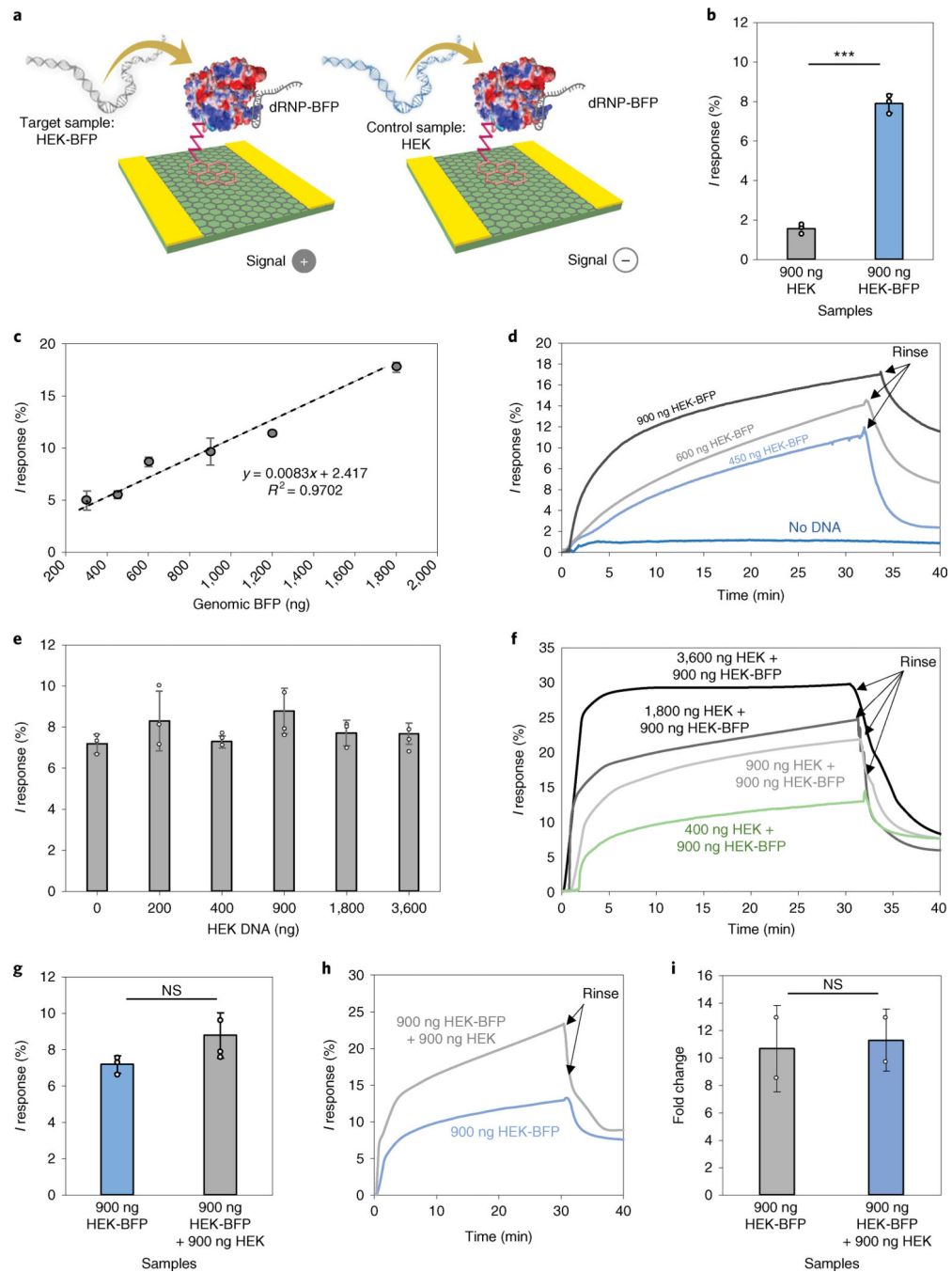


**Fig. 5 | CRISPR–Chip sensitivity and selectivity of the *bfp* target contained within whole genomic samples.**

**a.** Solutions of HEK-BFP (left) and HEK DNA (right) were analysed with the dRNP-BFP-functionalized CRISPR–Chip. **b.** CRISPR–Chip demonstrated a significant change in signal output (\*\* $P = 0.0002$ , two-tailed  $t$ -test) when exposed to target HEK-BFP, which contained the *bfp* sequence, compared with the genomic sample lacking the *bfp* target. **c.** CRISPR–Chip sensitivity calibration curve in the presence of varied amounts of HEK-BFP (mean;  $n = 3$ ).  $R^2$  is the determination coefficient. **d.** Real-time CRISPR–Chip  $I$  response in the

presence of varying concentrations of target HEK-BFP and the subsequent rinsing step (mean;  $n = 3$ ). **e**, CRISPR–Chip selectivity for 900 ng HEK-BFP in the presence of varied concentrations of HEK DNA lacking the *bfp* gene target (mean;  $n = 3$ ). **f**, Real-time CRISPR–Chip selectivity for 900 ng HEK-BFP in the presence of varied concentrations of HEK DNA lacking the *bfp* gene target (mean;  $n = 3$ ). **g**, CRISPR–Chip selectivity test (NS, not significant ( $P > 0.05$ ), two-tailed  $t$ -test) (mean;  $n = 3$ ). **h**, Real-time CRISPR–Chip selectivity test (mean;  $n = 3$ ). **i**, PCR selectivity normalized to the control ( $P > 0.05$ , two-tailed  $t$ -test). Error bars represent s.d.

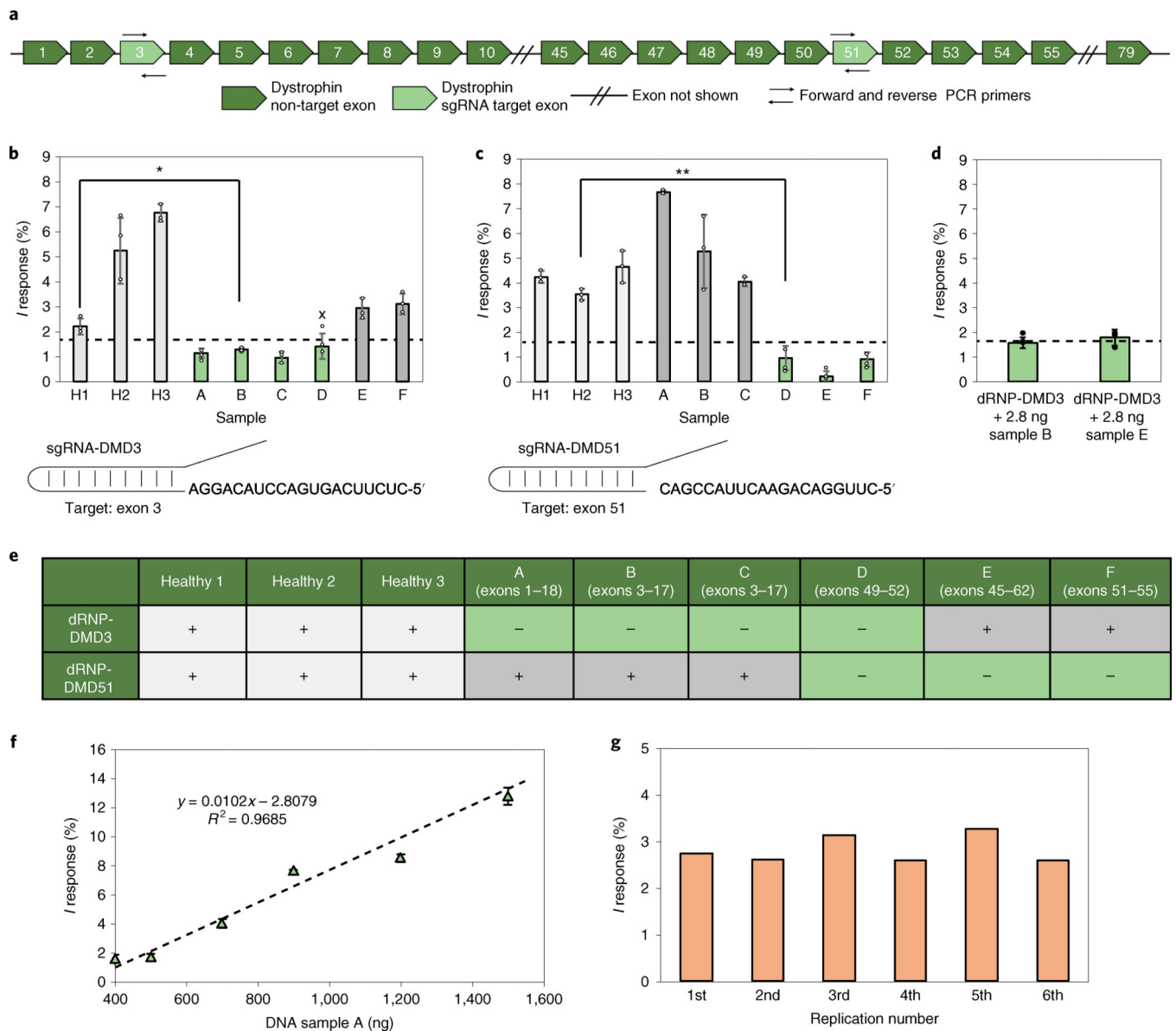


**Fig. 6 |. CRISPR–Chip analysis of healthy and DMD clinical samples for DMD-associated dystrophin exon deletions.**

**a**, Schematic of the dystrophin gene with highlighted target exons. **b**, Top,  $I$  response obtained by CRISPR–Chip functionalized with dRNP-DMD3 in the presence of healthy and DMD clinical samples ( $*P = 0.017$ , one-tailed  $t$ -test). Bottom, schematic of sgRNA-DMD3, designed to target exon 3.  $x$  represents a false negative as confirmed by sequencing. **c**, Top,  $I$  response obtained by CRISPR–Chip functionalized with dRNP-DMD51 in the presence of healthy and DMD clinical samples ( $**P = 0.0014$ , one-tailed  $t$ -test). Bottom, schematic of sgRNA-DMD51, designed to target exon 51. **d**, CRISPR–Chip’s negative signal threshold was defined by testing CRISPR–Chips with samples lacking target exons at the highest concentrations of genomic sample obtainable from commercially available buccal swabbing methods to ensure that high sample concentrations would not lead to false positives. **e**, CRISPR–Chip results for the presence of targeted exons (+) within healthy and DMD

clinical samples, as defined by a threshold of 1.73%. **f**, dRNP-DMD51-functionalized CRISPR–Chip’s *I* response in the presence of varied amounts of clinical sample A (mean;  $n = 3$ ). **g**, Reproducibility of individual CRISPR–Chips functionalized with dRNP-DMD51 in the presence of clinical sample A. Error bars represent s.d.

Author Manuscript

Author Manuscript

Author Manuscript

Author Manuscript